Published in final edited form as:
J Biol Chem. 2008 June 13; 283(24): 16830–16839.

Crystal Structure of Human Liver Δ⁴-3-Ketosteroid 5β-Reductase (Akr1d1) and Implications for Substrate Binding and Catalysis*

Luigi Di Costanzo§, **Jason E. Drury**†, **Trevor M. Penning**†, and **David W. Christianson**§

§*Roy and Diana Vagelos Laboratories, Department of Chemistry, University of Pennsylvania, Philadelphia, Pennsylvania 19104-6323*

†*Center of Excellence in Environmental Toxicology and Department of Pharmacology, University of Pennsylvania School of Medicine, Philadelphia, Pennsylvania 19104-6084*

Abstract

Aldo-Keto Reductase (AKR) 1D1 (steroid 5β-reductase) reduces all Δ^4-3-ketosteroids to form 5β-dihydrosteroids, a first step in the clearance of steroid hormones and an essential step in the synthesis of all bile acids. The reduction of the carbon-carbon double bond in an α,β-unsaturated ketone by 5β-reductase is a unique reaction in steroid enzymology, since hydride transfer from NADPH to the β-face of a Δ^4-3-ketosteroid yields a *cis*-A/B-ring configuration with a ~90° bend in steroid structure. Here, we report the first X-ray crystal structure of a mammalian steroid hormone carbon-carbon double bond reductase, human Δ^4-3-ketosteroid 5β-reductase (AKR1D1), and its complexes with intact substrates. We have determined the structures of AKR1D1 complexes with $NADP^+$ at 1.79 Å and at 1.35 Å (HEPES bound in active site) and with $NADP^+$ and cortisone at 1.90 Å resolution, $NADP^+$ and progesterone at 2.03 Å resolution, and with $NADP^+$ and testosterone at 1.62 Å resolution. Complexes with cortisone and progesterone reveal productive substrate binding orientations based on the proximity of each steroid carbon-carbon double bond to the *re*-face of the nicotinamide ring of $NADP^+$. This orientation would permit 4-pro-*R* hydride transfer from NADPH. Each steroid carbonyl accepts hydrogen bonds from catalytic residues Y58 and E120. The Y58F and E120A mutants are devoid of activity, supporting a role for this dyad in the catalytic mechanism. Intriguingly, testosterone binds nonproductively, thereby rationalizing the substrate inhibition observed with this particular steroid. The locations of disease-linked mutations thought to be responsible for bile acid deficiency are also revealed.

The Δ^4-3-ketosteroid functionality is present in all steroid hormones except estrogens. The first step in their metabolism involves the reduction of the Δ^4-ene to produce either 5α-dihydro- or 5β-dihydrosteroids in reactions catalyzed by steroid 5α-reductase or 5β-reductase, respectively (1). These two enzymes belong to distinct gene superfamilies (2,3) and structural information on these enzymes is currently lacking.

Δ^4-3-Ketosteroid 5β-reductase is a soluble monomeric NADPH dependent enzyme and a member of the aldo-keto reductase (AKR) superfamily, and in humans is designated AKR1D1

*This paper is dedicated to Dr. Paul Talalay, The John Jacob-Abel Distinguished Service Professor, Department of Pharmacology and Molecular Sciences at Johns Hopkins School of Medicine in honor of its 85th birthday. Paul has been a pioneer in steroid hormone enzymology throughout his career.

Address correspondence to: Dr. David W. Christianson, Roy and Diana Vagelos Laboratories, Department of Chemistry, University of Pennsylvania, Philadelphia, Pennsylvania 19104-6323; Tel: 215-898-5714; Fax: 215-573-2201; E-mail: chris@sas.upenn.edu; and Dr. Trevor M. Penning, Department of Pharmacology, University of Pennsylvania, 130C John Morgan Bldg., 3620 Hamilton Walk, Philadelphia, PA, 19104-6084. Phone: 215-898-9445; Fax: 215-573-2236; E-mail: penning@pharm.med.upenn.edu.

The atomic coordinates and structure factors of the AKR1D1-$NADP^+$-testosterone, AKR1D1-$NADP^+$-cortisone, AKR1D1-$NADP^+$-progesterone, AKR1D1-$NADP^+$-HEPES, and AKR1D1-$NADP^+$ complexes have been deposited in the Protein Data Bank with accession codes 3BUR, 3CMF, 3COT, 3BUV, and 3BV7, respectively.

(3,4). In utilizing NADPH as hydride donor the enzymatic reaction introduces a 90° bend at the steroid A/B ring junction, which adopts a *cis*-A/B or β-configuration (5-7) (Figure 1). In the absence of enzyme catalysis this reaction is extremely difficult to perform with chemical reductants. Treatment with borohydride favors formation of the 3β-allylic alcohol, and under harsher conditions the 3β,5α-tetrahydrosteroid is formed (8,9). It is only possible to generate a 5β-cholestane from the corresponding Δ^4-3-ketosteroid if a large directing group is placed at the C4 or C7 position to direct the face of hydride addition or catalytic hydrogenation (10, 11). Notably, AKR1D1 exclusively generates the reduced steroid bearing a thermodynamically less favorable 5β-configuration. Moreover, the enzyme only reduces the Δ^4-ene, leaving the 3-oxo group intact. Thus, AKR1D1 catalyzes a reaction that is unique in steroid enzymology and it accomplishes this with ease in comparison to chemical methods.

Rat Δ^4-3-ketosteroid 5β-reductase (AKR1D2) was first purified to homogeneity from liver as a 37 kDa protein (6). The cDNA for the corresponding human enzyme was cloned but only characterized in mammalian cell expression assays (3,12). Recently, this enzyme has been cloned and expressed in *E. coli* and completely characterized (13). These studies showed that a single enzyme could catalyze the reduction of C18-C27 Δ^4-3-ketosteroids yielding the corresponding 5β-dihydrosteroids. This enzyme thus plays an important role in the biosynthesis of bile acids (14-15). For example, AKR1D1 reduces Δ^4-cholesten-7α-ol-3-one and Δ^4-cholesten-7α,12α-diol-3-one to 5β-cholestan-7α-ol-3-one and 5β-cholestan-7α,12α-diol-3-one, respectively; in turn, these two 5β-dihydrosteroids yield the bile acid precursors 5β-cholestan-3α,7α-diol and 5β-cholestan-3α,7α,12α-triol in reactions catalyzed by 3α-hydroxysteroid dehydrogenases (HSDs) that belong to the same gene family, AKR1C1-AKR1C4 (4,15-17). Subsequent oxidation of the side-chain of 5β-cholestan-3α,7α-diol and 5β-cholestan-3α,7α,12α-triol yields the primary bile acids, chenodeoxycholate and cholic acid, respectively.

AKR1D1 deficiency results in accumulation of C_{27} bile acid precursors bearing intact Δ^4-3-oxo groups which upon reduction by steroid 5α-reductase can be converted to *allo*-bile acids (15,18). These sterols are hepatotoxic and their accumulation causes liver failure (19). Steroid 5β-reductase deficiency, which is characterized by single point mutations in the enzyme (L106F, P198L, P133R, and R261C) (20-22), is effectively treated with oral bile acid therapy (19). However, the effects of these mutations on enzyme structure and function remain to be delineated.

To date, the crystal structures of many of the human AKRs have been reported, including aldehyde reductase (AKR1A1) (23) and aldose reductase (AKR1B1) (24). The structures of relevant HSDs (AKR1C1-AKR1C4) have also been reported: AKR1C1, human 20α-hydroxysteroid dehydrogenase (25); AKR1C2, rat and human type III 3α-hydroxysteroid dehydrogenase/bile acid binding protein (26,27); AKR1C3, human type II 3α-hydroxysteroid dehydrogenase, type V 17β-hydroxysteroid dehydrogenase/prostaglandin F synthase (28); AKR1C4, human 3α-hydroxysteroid dehydrogenase type I (29); AKR1C5, rabbit 20α-hydroxysteroid dehydrogenase, type 3 (30); and AKR1C9, rat liver 3α-dihydroxysteroid dehydrogenase (31-33). Even though these HSDs share significant amino acid sequence identity, these crystal structures illuminate the roles of specific residues that contribute to the differing substrate specificities among these enzymes. All AKR structures to date contain a conserved catalytic tetrad of Y55, K84, H117, and D50 (numbering scheme based on AKR1C9, rat 3α-HSD). In contrast, AKR1D1 is the only AKR to have a modified catalytic tetrad: H117 is replaced by E120, and is proposed to play an important role in AKR1D1 catalysis (34). In addition to the above-mentioned HSD structures, the crystal structure of a novel short chain dehydrogenase/reductase, 5β-reductase from *D. lanata*, has been recently reported (35). However, this reductase is unrelated in that it adopts a Rossmann fold.

Here, we report the first X-ray crystal structure of a mammalian steroid hormone carbon-carbon double bond reductase, human Δ^4-3-ketosteroid 5β-reductase (AKR1D1). We have determined the structures of AKR1D1 complexed with $NADP^+$ at 1.79 Å resolution, $NADP^+$ and cortisone at 1.90 Å resolution, $NADP^+$ and progesterone at 2.03 Å resolution, and $NADP^+$ and testosterone at 1.62 Å resolution. Additionally, we report the crystal structures of the binary complex with $NADP^+$ at 1.35 Å resolution (containing a HEPES buffer molecule bound in the active site). These structures provide valuable inferences regarding the catalytic mechanism and also illuminate the possible effects of single point mutations responsible for bile acid deficiency.

Material And Methods

Materials

The vectors pET16b and pET28a were purchased from Novagen. *E. coli* strain C41 (DE3) was provided by Dr. J. E. Walker (MRC Laboratory of Molecular Biology, Cambridge, U.K.). The QuikChange II Site-Directed Mutagenesis kit was purchased from Stratagene. Restriction endonucleases were purchased from New England Biolabs. Synthetic oligonucleotides were obtained from Invitrogen (Life Technologies). NADPH was obtained from Roche. Steroids were purchased from Steraloids, Inc. [4-^{14}C]-Testosterone (50 mCi/mmol) was obtained from PerkinElmer Life and Analytical Sciences. Ni Sepharose 6 Fast flow was purchased from Amersham Biosciences. All other reagents were of ACS quality or higher.

Construction of Expression Vectors

Previously we reported the purification and characterization of recombinant AKR1D1 expressed from a pET16b-vector (13). This enzyme was refractory to crystallization and therefore a different expression vector was generated. The pET16b-AKR1D1 expression vector was digested with *Nde*I and *Bam*HI to remove the cDNA for AKR1D1. The resultant fragment was subcloned into the expression vector pET28a. The AKR1D1 insert was verified by dideoxysequencing.

The expression vectors for AKR1D1 Y58F and AKR1D1 E120A were made using the pET16b-AKR1D1 construct as a template by conducting site directed mutagenesis using the QuikChange method following the manufacturer's protocol. The following forward and reverse primers were used for the Y58F mutant, where the boldface nucleotides indicate the mutation introduced, 5′-dGGG GCC TAC ATC T**T**C CAA AAT GAA CAC GAA GTT GG-3′ and 5′-dCC AAC TTC GTG TTC ATT TTG G**A**A GAT GTA GGC CCC-3′, and for the E120A mutant the corresponding forward and reverse primers were: 5′-dG GAT CTT TAC ATC ATT G**C**A GTA CCA ATG GCC TTT AAG C-3′ and 5′-dG CTT AAA GGC CAT TGG T**A**C TGC AAT GAT GTA AAG ATC C-3′. The introduction of these mutations in the pET16b-AKR1D1 construct was verified by dideoxysequencing.

Expression and Purification of AKR1D1

The pET28a-AKR1D1 expression vector was used to transform competent *E. coli* C41 (DE3) cells. The cells were grown in 4 L cultures of Luria-Bertani media at 37 °C, containing 100 μg/mL ampicillin. Upon reaching A600 = 0.6, 1 mM IPTG was added to induce enzyme expression overnight. The following day the culture was centrifuged for 15 min at 10,000 g and the pellets were resuspended in 20 mM Tris/HCl (pH 7.9), 5 mM imidazole. Resuspensions were lysed by sonication, centrifuged for 15 min at 10,000 g, and the supernatant was dialyzed overnight in 20 mM Tris/HCl (pH 7.9), 20 mM imidazole, 0.5 M NaCl. The dialyzed fraction was loaded onto a Ni-Sepharose column equilibrated with the dialysis buffer and the column was washed with the same buffer. Bound protein was eluted with a linear gradient of 20-400 mM imidazole. Active fractions containing AKR1D1 were identified by monitoring the

conversion of [4-^{14}C]-testosterone to 5β-dihydrotestosterone (5β-DHT) by discontinuous assay using standard assay conditions and by visualization of the protein content of each fraction by SDS-PAGE. Peak fractions were pooled and dialyzed overnight in 20 mM Tris-HCl (pH 7.0), containing 1 mM EDTA, The final specific activity of the recombinant enzyme was 80 nmoles testosterone reduced/min/mg. The mutant proteins AKR1D1 Y58F and AKR1D1 E120A were purified in a similar manner.

Standard radiometric assay

The reduction of [4-^{14}C]-testosterone was used to monitor 5β-reductase activity collected during purification and for activity measurements. Reactions contained 2 μM [4-^{14}C]-testosterone (40,000 dpm), 8 μM cold testosterone, 5% acetonitrile and 100 mM potassium phosphate buffer, pH 6.0. Reactions were initiated by the addition of 200 μM NADPH and performed at 37 °C. Substrate and product of the quenched reaction were separated by TLC and quantitated by scintillation counting.

Crystallography

The ternary complexes of AKR1D1-NADP$^+$-testosterone, AKR1D1-NADP$^+$-cortisone, AKR1D1-NADP$^+$-progesterone, and AKR1D1-NADP$^+$-HEPES were crystallized by the hanging drop vapor diffusion method at 4 °C. In a typical experiment, drops containing 4.0 μL of enzyme solution [5.0 mg/mL AKR1D1, 2.0 mM NADP$^+$, 2.0 mM steroid, 10.0 mM Tris (pH 7.4)] and 4.0 μL of precipitant buffer [0.1 M HEPES/Tris-HCl (pH 7.0), 10-20% (wt/vol) PEG 4000, 10% iso-propanol] were equilibrated against a 1 mL reservoir of precipitant buffer. Diamond-like crystals appeared in approximately 2-3 days with typical dimensions of 0.2 mm × 0.3 mm × 0.5 mm. Crystals of each AKR1D1-NADP$^+$-steroid complex were further soaked for 1 week in the same mother liquor solution augmented with 5.0 mM NADP$^+$ and 5.0 mM steroid to insure complete ligand occupancy. Following transfer to a 28% glycerol cryoprotectant solution and flash-cooling, crystals of the AKR1D1-NADP$^+$-testosterone complex yielded diffraction data to 1.62 Å resolution at the Advanced Light Source (ALS) (beamline 8.2.2, λ=1.000 Å, 100 K). Diffraction intensities measured from these crystals indicated a space group $P2_12_12_1$ with unit cell parameters a = 49.8 Å, b = 110.1 Å and c = 129.4 Å. There were 2 molecules in the asymmetric unit and the Matthews coefficient V_M = 2.4 Å^3/Da, corresponding to a solvent content of 48.5%. Crystals of the AKR1D1-NADP$^+$-cortisone, AKR1D1-NADP$^+$-progesterone, and AKR1D1-NADP$^+$-HEPES complexes yielded diffraction data to 1.90 Å, 2.03 Å, and 1.35 Å resolution, respectively, at Brookhaven National Laboratory (beamlines X6A and X29A, λ=1.000 Å, 100 K) and were found to be isomorphous with crystals of the AKR1D1-NADP$^+$-testosterone complex (Table 1). Data reduction was achieved with HKL2000 (36) and Scalepack (36) (Table 1).

For crystallization of the AKR1D1-NADP$^+$ complex, hanging drops containing 4.0 μL of enzyme solution [5.0 mg/mL AKR1D1, 2 mM NADPH, 2.0 mM 5β-cholestan-3-one, 10.0 mM Tris (pH 7.4)] and 4.0 μL of precipitant buffer [0.1 M Tris/Hepes (pH 7.5), 10-20% (wt/vol) PEG 4000, 10% isopropanol] were equilibrated against a 1 mL reservoir of precipitant buffer. Crystals of the AKR1D1-NADP$^+$ complex were soaked for a week in the same mother liquor solution augmented with 5.0 mM 5β-cholestan-3-one, a steroid product containing a *cis*-A/B ring fusion. Following transfer to a cryoprotectant solution containing 28% glycerol, crystals of the AKR1D1-NADP$^+$ complex yielded diffraction data to 1.80 Å resolution at the Advanced Photon Source, Chicago (beamline BL 22-IM, λ=1.000 Å, 100 K) and were isomorphous with crystals of the ternary complexes discussed above (Table 1).

The structure of the AKR1D1-NADP$^+$-testosterone complex was solved by molecular replacement using one monomer of the AKR1C2-NADP$^+$-testosterone complex (PDB accession code 1J96 (27)) less the atoms of NADP$^+$ testosterone, and solvent as an initial search

probe. The program PHASER (37) was used to perform the molecular replacement calculations; the optimal solution for the positioning of the two monomers in the asymmetric unit yielded a total log-likelihood gain = 1832, a rotation function Z score (RFZ) = 12.3, and a translational function Z score (TFZ) = 19.5, for the first monomer, and RFZ = 13.2 and TFZ = 42.5 for the second monomer, using data in the 50 - 2.5 Å resolution range. The analysis of this solution showed reasonable packing interactions in the unit cell. The initial electron density map clearly revealed the presence of $NADP^+$ bound in the active site. Using the programs O (38) and CNS (39) for model fitting and refinement, respectively, the model was manually rebuilt and refined. In the later stages of refinement with CNS the noncrystallographic symmetry restraints were released, after which the program SHELX was used to complete the refinement (40). Additional solvent molecules were introduced during refinement with SHELX and the electron density map of testosterone became very clearly defined. In the final stage of refinement, the atomic coordinates of testosterone were retrieved from entry TESTOM in the Cambridge Structural Database (41), built into the electron density map, and refined with full occupancy. The quality of the final model was checked with Verify3d (42); the analysis of the structure was performed with PISA (43).

The crystal structures of the AKR1D1-$NADP^+$-cortisone, AKR1D1-$NADP^+$-progesterone, AKR1D1-$NADP^+$-HEPES and AKR1D1-$NADP^+$ complexes were solved by the difference Fourier method. Refinement was performed as described above using CNS (39).

Twenty-one residues at the N-terminus (the uncleaved expression tag from the PET28a vector) were disordered and therefore excluded from the final model of each structure. The exclusion of 21/347 residues in each monomer (6.1% of the scattering matter) likely contributed to the slightly elevated R and R_{free} values recorded in Table 1.

Results

Crystal structure of the AKR1D1-$NADP^+$ complex

The asymmetric unit of the unit cell contains two monomers of AKR1D1. Each monomer consists of a 325-residue polypeptide chain that adopts an $(\alpha/\beta)_8$-barrel fold typical of AKRs. The top of the β-barrel is capped by loops A (I119-L147), B (Y219-L238), and C (L302-Y326), which enclose the active site (Figure 2a). Notably, the P133-K139 segment in loop A of monomer A exhibits higher thermal B factors compared with the P133-K139 segment in monomer B, where this segment appears to be stabilized in part by interlattice contacts. However, the loop A conformations in monomers A and B are essentially identical (data not shown).

Given the amino acid sequence identities of 56 % between AKR1D1 and AKR1C2 (27) and 58 % between AKR1D1 and AKR1C9 (33), the overall tertiary structures of these enzymes are quite similar. The root-mean-square (r.m.s.) deviation of 307 Cα atoms between AKR1D1 in complex with $NADP^+$ and AKR1C2 in complex with $NADP^+$ and testosterone (PDB code 1J96) (27) is 1.0 Å, and is 0.78 Å for 317 Cα atoms between AKR1D1 and AKR1C9 complexed with $NADP^+$ and testosterone (PDB code 1AFS) (33). However, significant conformational differences of loops A, B and C are observed when the structures of AKR1D1, AKR1C2, and AKR1C9 are compared (Figure 2b). The majority of amino acid substitutions between AKR1D1 and these enzymes are found in these loops. The V309 - F322 segment of loop C and its corresponding segment in AKR1C2 exhibit significant Cα deviations of ~4 Å. Since these loops play an important role in substrate binding, it is likely that their sequence and structural differences reflect differences in steroid substrate specificity and catalysis among these enzymes.

The $NADP^+$ cofactor in the AKR1D1-$NADP^+$ complex adopts an extended *anti*-conformation as observed in other AKR structures and is located in a long tunnel with the adenine group exposed to solvent and the nicotinamide ring located deep inside the tunnel oriented toward the central active site cavity (Figure 2a). Approximately 84% of the accessible surface area of $NADP^+$ is buried inside the tunnel. The $NADP^+$ cofactor participates in a significant number of hydrogen bond interactions (Figure 3). Notably, the cofactor binding mode is essentially conserved with respect to that observed in AKR1C9 (32) or AKR1C2 (27). In complex with AKR1D1, the nicotinamide head group of $NADP^+$ is stacked against Y219, and the carboxamide group makes contacts with N170, S169 and Q193. Additionally, the phosphate group of 2′-AMP makes an electrostatic link with R279. However, these structures do not reveal a hydrogen bond interaction between N227 and K34 or K273 that would correspond to the salt link interaction between D217 and K263 observed in the AKR1A1 structure (23) or the salt link interactions between D216 and K21 and K262 observed in the AKR1B1 structure (24). These salt links create a “safety-belt” that contributes to the high affinity (~10 nM) of cofactor binding to AKR1A1 and AKR1B1. Since $NADP^+$ binding to AKR1D1 lacks this “safety belt”, binding affinity should be weaker and more comparable to cofactor binding to AKRs similarly lacking a “safety belt” (100-200 nM), and this is what is observed (13).

Interestingly, when crystals of the AKR1D1-$NADP^+$ complex are grown in the presence of 5β-cholestan-3-one, the binding of this product-like steroid containing a *cis*-A/B ring fusion is not observed. Instead, either a molecule of glycerol from the cryoprotectant solution binds in the active site of monomer A (1.79 Å resolution structure; data not shown), or a HEPES molecule from the crystallization buffer binds in the active site of monomer B (1.35 Å resolution structure; Figure 3). Thus, these two structures represent those of the binary AKR1D1-$NADP^+$ complex.

Crystal structures of the AKR1D1-$NADP^+$-cortisone and AKR1D1-$NADP^+$-progesterone complexes

In these enzyme-substrate complexes, the electron density of each steroid substrate is clear and unambiguous (Figures 4a and 4b), showing that each steroid lies perpendicular to the $NADP^+$ cofactor. The binding of cortisone is very similar to the binding of progesterone even though these steroids bear different pendant groups on their D rings.

Overall, the crystal structure of each ternary complex is very similar to that of the AKR1D1-$NADP^+$ complex, with r.m.s. deviations of 0.26 Å and 0.13 Å, respectively, for 325 Cα atoms. However, important conformational differences are evident in loops A and B. Significantly, cortisone and progesterone binding trigger the movement of S225-V231 in loop B away from the active site, with Cα deviations ranging 0.3-2 Å. Furthermore, a ~7 Å movement of the side chain of W230 accommodates substrate binding (illustrated for cortisone binding in Figure 5). Thus, W230 appears to play a key role in packing against the β-face of the steroid ring system in the active site of human AKR1D1, as also observed for the corresponding tryptophan residue in the structure of the AKR1C9-$NADP^+$-testosterone complex (33).

In the AKR1D1 active site, approximately 80% of the accessible surface area of each steroid substrate is buried in the hydrophobic binding pocket. Each steroid substrate is positioned with its β-face oriented towards the *re*-face of the nicotinamide ring of $NADP^+$ such that the steroid carbon-carbon double bond would be adjacent to the 4-pro-*R* hydrogen of NADPH (Figures 4a and 4b). The C3 carbonyl oxygen of each steroid substrate accepts hydrogen bonds from the phenolic hydroxyl group of Y58 and the *anti*-oriented conformer of the carboxylic acid side chain of E120. Notably, the C3 carbonyl oxygen of each substrate occupies the same position as the water molecule that hydrogen bonds with Y58 and E120 in the AKR1D1-$NADP^+$ complex (Figures 2 and 3). Site-directed mutagenesis of these residues to Y58F and E120A supports their role in catalysis since neither mutant has any detectable activity in the

reduction of testosterone using the standard radiometric assay where the limit of detection is 0.002 nmoles/min.

Crystal structure of the AKR1D1-NADP$^+$-testosterone complex

In this enzyme-substrate complex, the electron density of testosterone is extremely well defined. However, the arrangement of NADP+ and testosterone differ from that seen in the other ternary complexes since they are parallel and not perpendicular. Testosterone also binds with a "backward" orientation in which its D-ring binds in the same region occupied by the A-rings of cortisone and progesterone in their respective complexes with AKR1D1 (Figure 4c). Consequently, the carbon-carbon double bond of testosterone is distant from the nicotinamide ring of the cofactor, and this binding orientation is judged to be nonproductive. The side chain of W230 does not undergo a conformational change to accommodate testosterone binding, and instead remains in the conformation observed in the structure of the substrate-free AKR1D1-NADP$^+$ complex (Figure 5). Approximately 85% of the accessible surface area of testosterone is buried in the hydrophobic binding pocket. The testosterone C3 carbonyl group accepts hydrogen bonds from N227 and S225, while the testosterone hydroxyl group makes a hydrogen bond interaction with Y132.

Nonproductive testosterone binding modes observed with AKR1C2 and AKR1D1 suggest that this particular steroid can occupy more than one position and that at high steroid concentrations used in the crystallization trials the nonproductive binding mode is favored. This is reflected in substrate inhibition observed with AKR1C2 (44,45). We also observe substrate inhibition of AKR1D1 by high concentrations of testosterone. While the K_m value for this steroid is close to 2.0 μM, concentrations of testosterone that exceed 10 μM produce marked inhibition (Figure 6).

Disease-Linked Mutations

Four point mutations in AKR1D1 are associated with bile acid deficiency: L106F, P198L, P133R, and R261C (20-22). As predicted from other AKR structures, these residues are not located in the cofactor or steroid binding sites nor are they involved in catalysis. The locations of these residues in the AKR1D1 structure are shown in Figure 7. The P133R substitution in the A loop is closest to the substrate binding site, and it is conceivable that this substitution perturbs the conformational changes of the A loop that accompany steroid binding. The remaining mutations may exert a deleterious effect on catalysis by causing structural changes that propagate through the protein scaffold to perturb substrate and/or cofactor binding, or by otherwise destabilizing the folded conformation of the protein.

Discussion

The X-ray crystal structure of human Δ^4-3-ketosteroid 5β-reductase (AKR1D1) is the first structure of a mammalian steroid carbon-carbon double bond reductase, As a member of the AKR superfamily it is not surprising that the $(\alpha/\beta)_8$-barrel fold and the NADP$^+$ cofactor binding site of AKR1D1 are highly conserved with those other members of the superfamily. However, the structures of AKR1D1-substrate complexes reported herein illuminate new features of steroid substrate recognition, the catalytic mechanism, and the positions of natural mutations associated with bile acid deficiency.

Substrate Recognition

AKR1D1 binds Δ^4-3-ketosteroids productively and non-productively. In the productive binding mode observed with cortisone and progesterone, the two substrates are bound similarly in a pocket defined by residues from the β2-α2 loop, loop A, loop B, and loop C. Alignments of pocket and loop residues of AKR1D1 with those of other AKR1C structures containing

bound steroids are shown in Tables S1 and S2 in the Supporting Information. Of the ten pocket residues assigned, Y58 is catalytic and Y26 and W230 are highly conserved. The indole ring of W230 in the AKR1D1 structures is versatile in that rotation around both side chain torsion angles and movement of the associated polypeptide backbone of loop B allows the indole ring to pack differently, i.e., against the β-face of a productively bound steroid substrate or against the α-face of a nonproductively bound steroid substrate (Figure 5).

Interestingly, superposition of the AKR1D1-$NADP^+$-cortisone and AKR1C9-$NADP^+$-testosterone complexes, in which both substrates adopt productive binding orientations, reveals that the substrate is immobilized more deeply in the active site of AKR1D1 compared with AKR1C9 (Figure 8). In part, this appears to result from the removal of the steric bulk of the H120 imidazole side chain by the substitution of E120 in AKR1D1. As a result, the 4-pro-*R* hydride of the NADPH cofactor would be adjacent to the substrate C3 carbonyl group in the AKR1C9 active site, and the 4-pro-*R* hydride of the NADPH cofactor would be adjacent to C5 of the substrate carbon-carbon double bond in the AKR1D1 active site (Figure 8).

Catalytic Mechanism

The four catalytic residues D53, Y58, K87 and E120 are located in the center of the β-barrel (Figure 2a). The side chain of K87 donates hydrogen bonds to D53 and Y58. In the substrate-free enzyme, the phenolic hydroxyl group of Y58 donates a hydrogen bond to a water molecule, which in turn hydrogen bonds with E120. Since the C3 carbonyl oxygen atoms of substrates cortisone and progesterone displace this water molecule in their complexes with AKR1D1, the side chain of E120 must be protonated as the *anti*-oriented carboxylic acid in order to donate a hydrogen bond to the substrate carbonyl oxygen (and possibly also the water molecule in the substrate-free enzyme). Furthermore, given that carboxylate groups that serve as general bases generally do so with their more basic, *syn*-oriented lone electron pairs (46), it is reasonable to conclude that protonated carboxylic acids that serve as general acids or hydrogen bond donors may do so with their more acidic (pKa ~ 0.5) *anti*-oriented conformers. Thus, in AKR1D1, the *anti*-oriented conformer of E120 may serve as a superacidic hydrogen bond donor to help activate the α,β-unsaturated ketone moiety of the substrate for carbon-carbon bond reduction by NADPH.

That E120 appears in AKR1D1 represents a unique exception for AKRs having an $(\alpha/\beta)_8$ fold. All other AKRs including AKR1C9 (33) and AKR1C2 (26), have a histidine residue at the corresponding position. The side chain conformations of D53, Y58, K87 are mostly conserved with respect to the conformations of corresponding residues in the AKR1C2-$NADP^+$-testosterone complex; the side chain of E120 is coplanar with respect to the orientation of the corresponding histidine residue in this complex (27). Interestingly, the hydrogen bonded water molecule between Y58 and E120 occupies a position close to that of an acetate oxygen atom observed in the AKR1C2-$NADP^+$-testosterone complex (27), and a corresponding water molecule is also observed in the crystal structure of AKR1C9 (32). It is proposed that the binding of this water molecule in AKR1C9 mimics the binding of the carbonyl oxygen of a 3-ketosteroid substrate (33).

In AKR1D1, the interactions of Y58 and E120 with the carbonyl groups of steroid substrates suggest that both residues participate in the catalytic mechanism of carbon-carbon double bond reduction. In AKR1B1 and AKR1C9, site-directed mutagenesis studies provide compelling evidence that the catalytic tyrosine acts as the general acid-base (47,48). Moreover, site-directed mutagenesis studies of AKR1C9 also show that the corresponding H117E substitution introduces 5β-reductase activity into this enzyme (34). Based on k_{cat} and k_{cat}/K_m pH-rate profiles for wild-type and H117E AKR1C9 enzymes, a facilitatory role for the glutamic acid residue is proposed in which it alters the pK of Y55, which functions as the general acid. This facilitatory role is based on an acid-shift of the pK_b of Y55 in the H117E mutant. These data

are interpreted to indicate that Y55 has more $TyrOH_2^+$ character (i.e., it may behave as a "superacid"), which in turn polarizes the α,β-unsaturated ketone so that hydride transfer can occur at C5.

The carboxylic acid side chain of E120 may also serve as a "superacid" to help polarize the C3 ketone of a productively bound substrate such as cortisone or progesterone (Figures 4a and 4b). The nonenzymatic mechanism of carbon-carbon double bond reduction in an α,β-unsaturated ketone requires a superacid such as $HF\text{-}SbF_5$ (49), and it is possible that AKR1D1 adopts a similar strategy for catalysis. Generation of the AKR1D1 Y58F and E120A mutants abolishes all enzyme activity, consistent with the crucial role of these residues in catalysis. Once 4-pro-*R* hydride transfer from the *re*-face of NADPH to the carbon-carbon double bond of the substrate is achieved, the substrate will adopt a bent, *cis*-A/B ring conformation. Either an enzyme-bound residue or a solvent molecule will protonate the C4 atom of the substrate in the final step of the steroid reduction reaction. A proposed mechanism that incorporates these structural data in light of available enzymological measurements is presented in Figure 9.

Disease-linked mutations

The four point mutations associated with inherited bile acid deficiency are located in regions independent of substrate recognition and catalysis. If these mutations are responsible for bile acid deficiency then it is likely that they affect conformational changes in loop A that accompany substrate binding (P133R) and/or otherwise compromise enzyme stability. Future studies of these mutant recombinant proteins and their expression in mammalian cells will allow us to probe the structural and functional consequences of these mutations.

Supplementary Material

Refer to Web version on PubMed Central for supplementary material.

Acknowledgements

This work was supported by NIH research grants R01-GM56838 to D.W.C. and R01-DK47015 and P30 ES013508 to T.M.P.

We thank the Brookhaven National Laboratory (beamlines X6A, X12B and X29A), Upton, New York, the Advanced Light Source (beamline 8.2.2), Berkeley, California, and Advanced Photon Source (beamline IM-22), Chicago, Illinois, for beamtime access.

References

1. Tomkins G. Rec Prog Horm Res 1956;12:125–133.
2. Russell DW, Wilson JD. Ann Rev Biochem 1994;63:25–61. [PubMed: 7979239]
3. Kondo KH, Kai MH, Setoguchi Y, Eggersten G, Sjöblom P, Setoguchi Y, Okuda KI, Björkhem J. Eur J Biochem 1994;219:357–363. [PubMed: 7508385]
4. Jez JM, Bennett MJ, Schelgel BP, Lewis M, Penning TM. Biochem J 1997;325:625–636. [PubMed: 9307009]
5. Berséus O, Danielsson H, Einarsson K. J Biol Chem 1967;242:1211–1219. [PubMed: 4381551]
6. Okuda K, Okuda K. J Biol Chem 1984;259:7519–7524. [PubMed: 6736016]
7. Onishi Y, Noshiro M, Shimosato T, Okuda K. FEBS Lett 1991;283:215–218. [PubMed: 1710579]
8. Norymberski JK, Woods GF. J Chem Soc 1955:3426–3430.
9. March, J. Advanced Organic Chemistry: Reactions, Mechanisms and Structure. John Wiley & Sons; New York, NY: 1984. p. 694-695.
10. Michalak K, Stepanenko W, Wicha J. R Soc Chem Perkin 2000;1:1587–1594.
11. Takeda K, Osaka H, Akio H, Shionogi, et al. YakugakuZasski 1961;81:325–30.
12. Charbonneau A, Luu-The V. Biochim Biophys Acta 2001;1517:228–235. [PubMed: 11342103]

13. Drury, JE.; Penning, TM. Enzymology and Molecular Biology of Carbonyl Metabolism. Weiner, H.; Maser, E.; Lindhal, R.; Plapp, B., editors. Purdue University Press; West Lafayette, IN: 2007. p. 332-340.
14. Russell DW, Setchell KD. Biochemistry 1992;31:4737–4749. [PubMed: 1591235]
15. Russell DW. Ann Rev Biochem 2003;72:137–174. [PubMed: 12543708]
16. Penning TM, Burczynski ME, Jez JM, Hung CF, Lin HK, Ma H, Moore M, Palackal N, Ratnam K. Biochem J 2000;351:67–77. [PubMed: 10998348]
17. Deyashiki Y, Taniguchi H, Amano T, Nakayama T, Hara A, Sawada H. Biochem J 1992;282:741–746. [PubMed: 1554355]
18. Setchell KD, Suchy FJ, Welsh MB, Zimmer-Nechemias L, Heubi J, Balistreri WF. J Clin Invest 1988;82:2148–2157. [PubMed: 3198770]
19. Clayton PT, Mills KA, Johnson AW, Barabino A, Marazzi MG. Gut 1996;38:623–628. [PubMed: 8707100]
20. Kimura A, Kondo KH, Okuda KI, Higashi S, Suzuki M, Kurosawa T, Tohma M, Inoue T, Nishiyori A, Yoshino M, Kato H, Setoguchi T. Eur J Pediatr 1998;157:386–390. [PubMed: 9625335]
21. Gonzales E, Cresteil D, Baussan C, Dabadie A, Gerhardt MF, Jacquemin E. J Hepatology 2004;40:716–718.
22. Lemonde HA, Custard EJ, Bouquet J, Duran M, Overmars H, Scambler PJ, Clayton PT. Gut 2003;52:1494–1499. [PubMed: 12970144]
23. El-Kabbani O, Green NC, Lin G, Carson M, Narayana SV, Moore KM, Flynn TG, DeLucas LJ. Acta Crystallogr Sect D: Biol Crystallogr 1994;50:859–868. [PubMed: 15299353]
24. Wilson DK, Bohren KM, Gabbay KH, Quiocho FA. Science 1992;257:81–84. [PubMed: 1621098]
25. Couture JF, Legrand P, Cantin L, Luu-The V, Labrie F, Breton R. J Mol Biol 2003;331:593–604. [PubMed: 12899831]
26. Jin Y, Stayrook SE, Albert RH, Palackal NT, Penning TM, Lewis M. Biochemistry 2001;40:10161–10168. [PubMed: 11513593]
27. Nahoum V, Gangloff A, Legrand P, Zhu DW, Cantin L, Zhorov BS, Luu-The V, Labrie F, Breton R, Lin SX. J Biol Chem 2001;276:42091–42098. [PubMed: 11514561]
28. Komoto J, Yamada T, Watanabe K, Takusagawa F. Biochemistry 2004;43:2188–2198. [PubMed: 14979715]
29. Ugochukwu E, Smee C, Guo K, Lukacik P, Kavanagh K, Debreczeni JE, von Delft F, Weigelt J, Sundstrom M, Arrowsmith C, Edwards A, Oppermann U. To be Published. PDB accession code 2FVL
30. Couture JF, Legrand P, Cantin L, Labrie F, Luu-The V, Breton R. J Mol Biol 2004;339:89–102. [PubMed: 15123423]
31. Hoog SS, Pawlowski JE, Alzari PM, Penning TM, Lewis M. Proc Natl Acad Sci U S A 1994;91:2517–2521. [PubMed: 8146147]
32. Bennett MJ, Schlegel BP, Jez JM, Penning TM, Lewis M. Biochemistry 1996;35:10702–10711. [PubMed: 8718859]
33. Bennett MJ, Albert RH, Jez JM, Ma H, Penning TM, Lewis M. Structure 1997;5:799–812. [PubMed: 9261071]
34. Jez JM, Penning TM. Biochemistry 1998;37:9695–9703. [PubMed: 9657682]
35. Thorn A, Egerer-Sieber C, Jäeger CM, Herl V, Müeller-Uri F, Kreis W, Muller YA. J Biol Chem. 2007In press. Manuscript jbc.M706185200
36. Otwinowski Z, Minor M. Methods Enzymol 1997;276:307–326.
37. McCoy AJ, Grosse-kunstleve RW, Storni LC, Read RJ. Acta Crystallogr Sect D: Biol Crystallogr 2005;61:458–464. [PubMed: 15805601]
38. Jones TA, Zou JY, Cowan SW, Kjeldgaard M. Acta Crystallogr Sect A: Found Crystallogr 1991;47:110–119.
39. Brünger AT, Adams PD, Clore GM, DeLano WL, Gros P, Grosse-Kunstleve RW, Jiang JS, Kuszewski J, Nilges M, Pannu NS, Read RJ, Rice LM, Simonson T, Warren GL. Acta Crystallogr Sect D: Biol Crystallogr 1998;54:905–921. [PubMed: 9757107]

40. Sheldrick G, Schneider T. Methods Enzymol 1997;277:319–343. [PubMed: 18488315]
41. Allen FH. Acta Crystallogr Sect D: Biol Crystallogr 2002;58:380–388.
42. Eisenberg D, Lüthy R, Bowie JU. Methods Enzymol 1997;277:396–404. [PubMed: 9379925]
43. Krissinel E, Henrick K. J Mol Biol 2007;372:774–797. [PubMed: 17681537]
44. Steckelbroeck S, Jin Y, Oyesanmi B, Kloosterboer HJ, Penning TM. Mol Pharmacol 2004;66:1702–1711. [PubMed: 15383625]
45. Jin Y, Penning TM. Steroids 2006;71:380–91. [PubMed: 16455123]
46. Gandour R. Bioorg Chem 1981;10:169–176.
47. Grimshaw CE, Bohren KM, Lai CJ, Gabbay KH. Biochemistry 1995;34:14374–14384. [PubMed: 7578041]
48. Schlegel BP, Jez JM, Penning TM. Biochemistry 1998;37:3538–3548. [PubMed: 9521675]
49. Coustard JM, Douteau MH, Jacquesy JC, Jacquesy R. Tetrahedron Lett 1975;25:2029–2030.
50. Laskowski RA, MacArthur MW, Moss DS, Thornton JM. J Appl Crystallogr 1993;26:283–291.

Abbreviations used

AKR1D1
: Δ^4-3-ketosteroid 5β-reductase

HSD
: hydroxysteroid dehydrogenases

AKR
: aldo-keto reductases

HEPES
: 4-(2-hydroxyethyl)-1-piperazineethanesulfonic acid

5β-DHT
: 5β-dihydrotestosterone

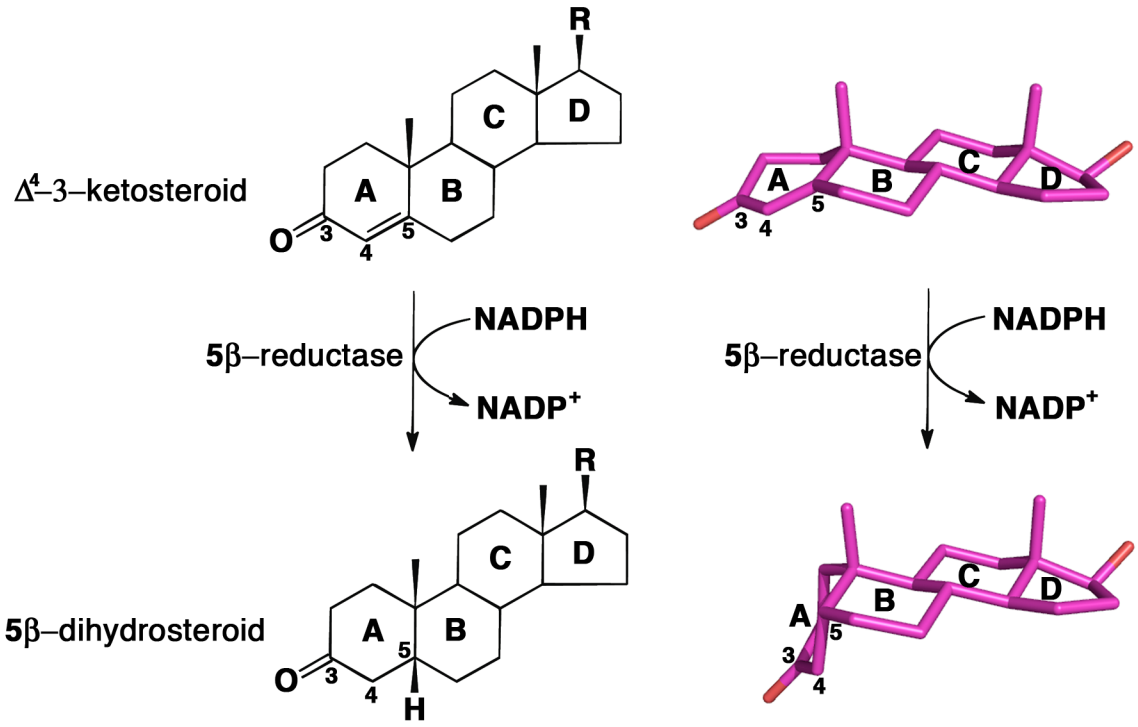

FIGURE 1.

Reduction of the carbon-carbon double bond at position C5 of a Δ^4-3-ketosteroid to form a 5β-dihydrosteroid as catalyzed by AKR1D1. Steroid rings and selected carbon atoms are labeled according to standard steroid nomenclature. The structures of testosterone and 5β-dihydrotestosterone (R = OH) illustrate the remarkable configurational differences between the substrate and product of this reaction (atomic coordinates retrieved from Cambridge Structural Database (CSD) entries TESTOM and JEPJET, respectively (41)).

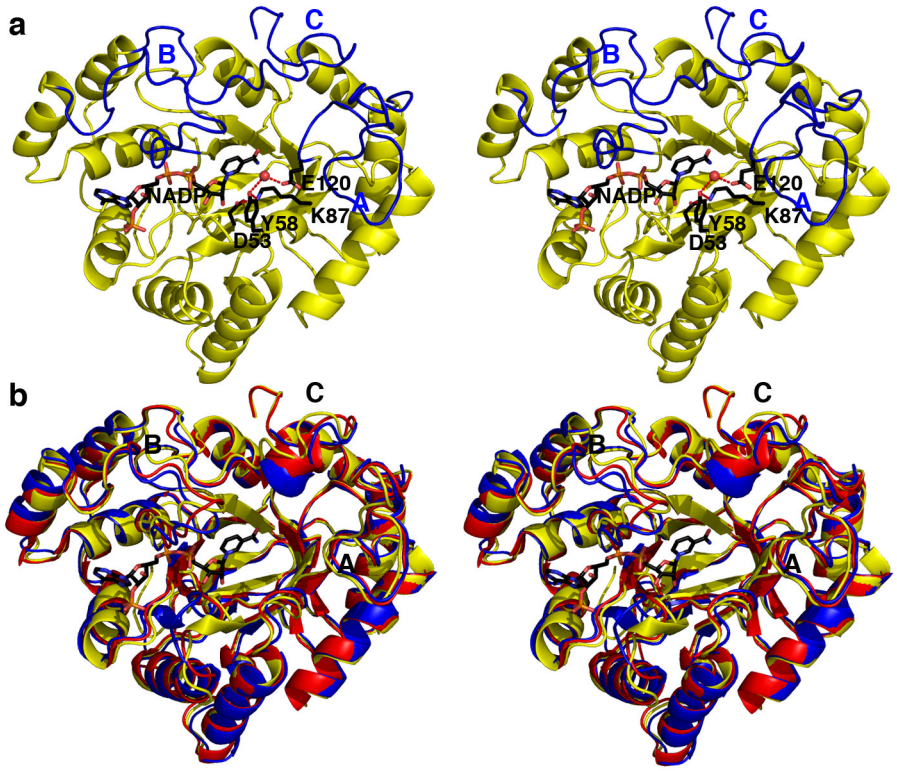

FIGURE 2. AKR1D1-NADP$^+$ complex

(a) AKR1D1 adopts the $(\alpha/\beta)_8$ fold conserved among members of the AKR superfamily. Loops A, B and C (blue) flank the steroid binding pocket. Atoms of the catalytic tetrad and NADP$^+$ are labeled and color coded as follows: carbon, black; oxygen, red; nitrogen, blue. The water molecule hydrogen bonded between E120 and Y58 is indicated by a red sphere. Hydrogen bonds are indicated by red dashed lines. (b) Superposition of AKR1D1 (yellow), AKR1C9 (red), and AKR1C2 (blue) reveals significant conformational differences in loops A, B, and C.

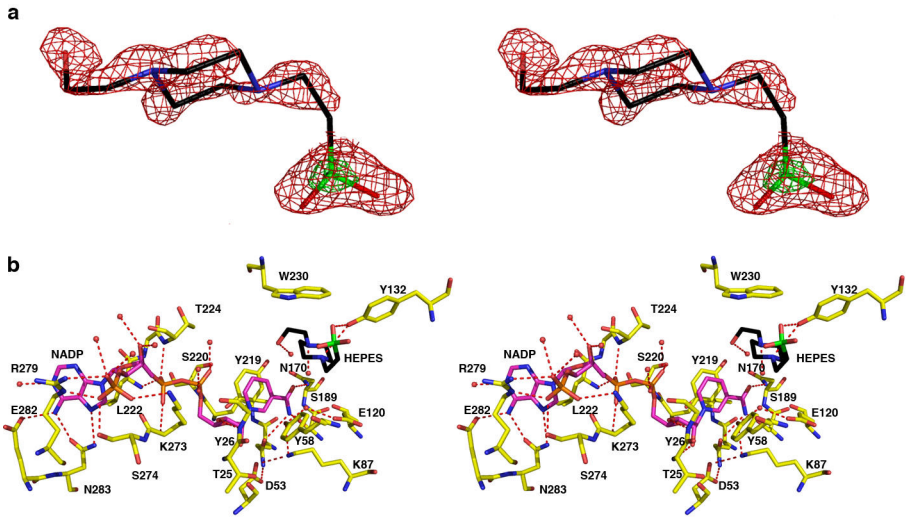

FIGURE 3. AKR1D1-NADP$^+$-HEPES complex

(a) Difference electron density map of HEPES bound in the active site of AKR1D1 prior to the inclusion of HEPES in the refinement (contoured at 2.2σ, red). The electron rich sulfur atom of HEPES is indicated by its stronger electron density contoured at 6.7σ (green). (b) Hydrogen bond interactions in the AKR1D1-NADP$^+$-HEPES complex are indicated by red dashed lines. Atoms are color coded as in Figure 2a except that protein carbon atoms are yellow, HEPES carbon atoms are black and its sulfur atom is green.

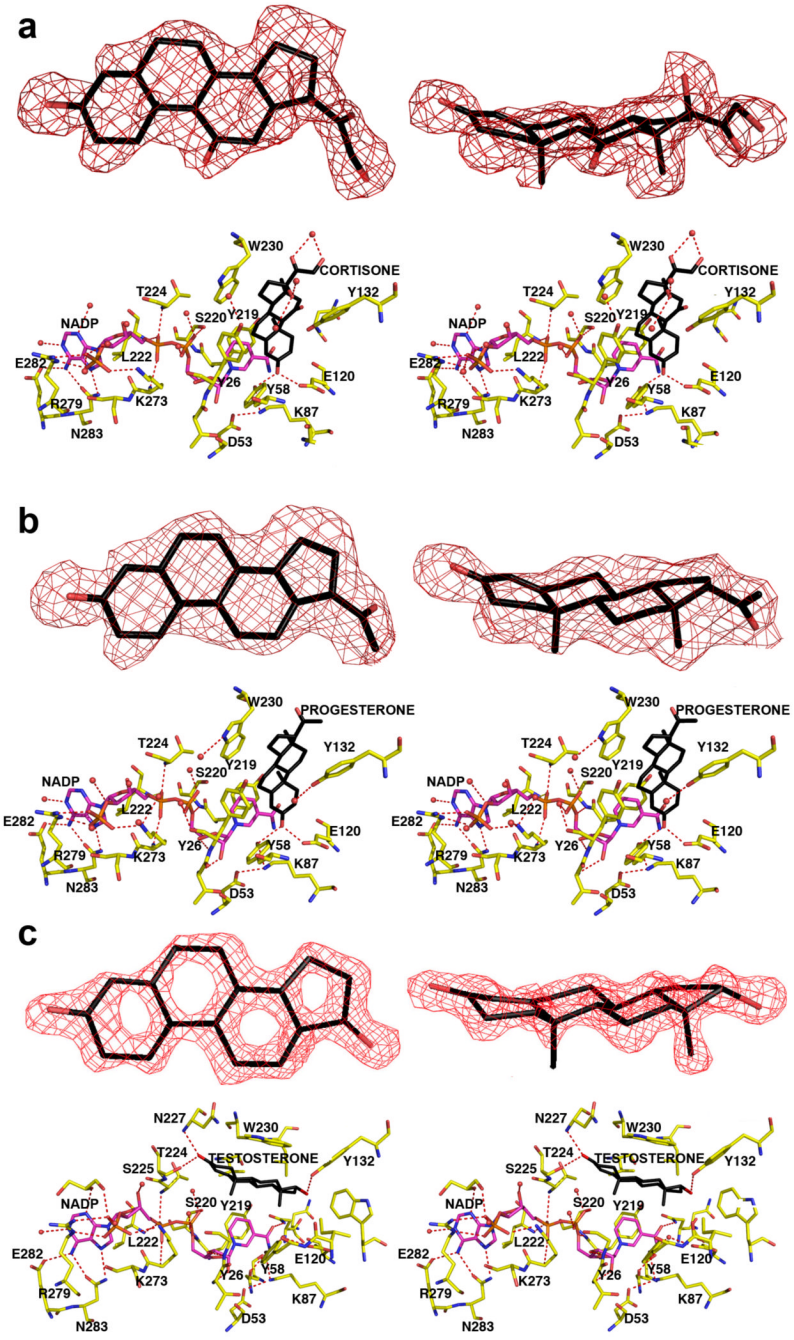

FIGURE 4. AKR1D1-NADP$^+$-steroid complexes

Two map orientations are shown for each steroid, and hydrogen bond interactions are indicated by red dashed lines. Atoms are color coded as in Figure 2a except that protein carbon atoms are yellow. For clarity, the orientation of the protein is rotated ~180° horizontally relative to the orientation shown in Figure 2a. (a) Difference electron density map of cortisone contoured at 2.7σ. (b) Difference electron density map of progesterone contoured at 2.6σ. (c) Difference electron density map of testosterone contoured at 2.3σ. Note the dramatically different, nonproductive binding mode of testosterone; in contrast with the binding of cortisone and

progesterone, the A-ring of testosterone is oriented away from the catalytic tetrad and the nicotinamide ring of the cofactor.

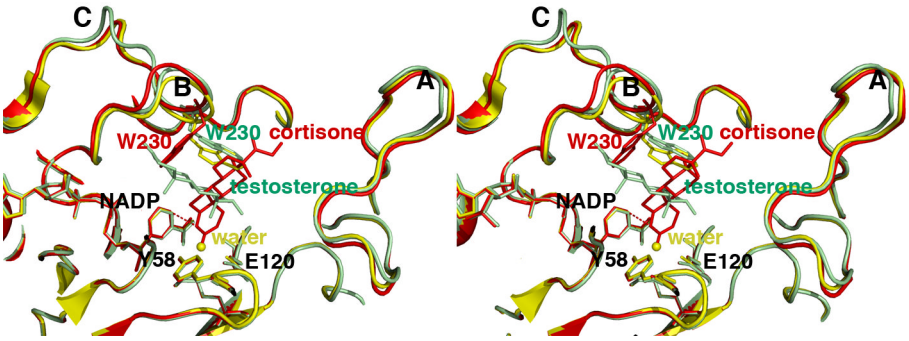

FIGURE 5. Least-squares superposition of the AKR1D1-NADP$^+$ complex (yellow), the AKR1D1-NADP$^+$-cortisone complex (red), and the AKR1D1-NADP$^+$-testosterone complex (green)

The distance of ~3.7 Å between the anomeric carbon of NADP$^+$ and the olefinic carbon C4 of cortisone is indicated by a red dashed line, which would represent the trajectory of hydride transfer from NADPH. The position of the water molecule in the unliganded structure is indicated by a yellow sphere. Loops A, B, and C are labeled; note that loop B and W230 in particular must undergo a significant conformational change to accommodate productive substrate binding as represented by cortisone (red). The indole ring of W230 remains in its substrate free conformation (yellow) to accommodate the nonproductive binding mode of testosterone (green).

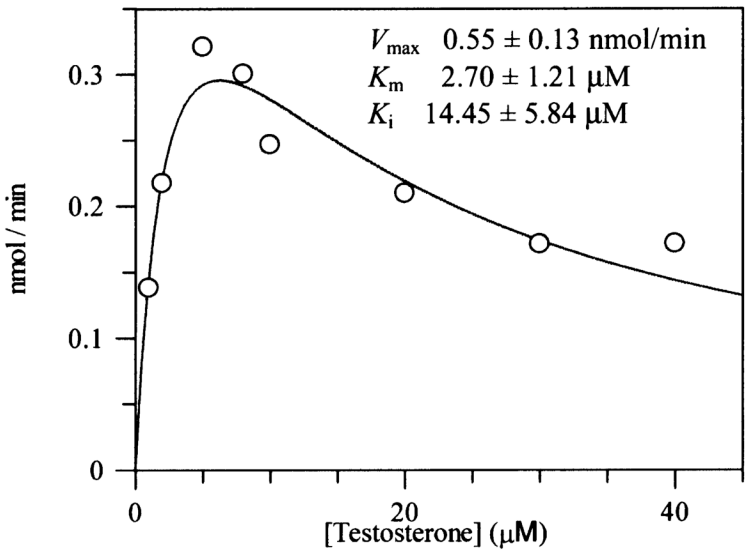

FIGURE 6. Substrate inhibition of AKR1D1 by testosterone

Velocity versus substrate plot for AKR1D1 showing substrate inhibition using testosterone. Assays contained 0.078 μM enzyme, 1 - 40 μM testosterone, 15 μM NADPH, 4% acetonitrile in 100 mM potassium phosphate buffer, pH 6.0, in a final volume of 1 mL. Reactions were monitored fluorimetrically by using an excitation wavelength of 340 nm (slit-width 5 nm) and an emission wavelength set at 450 nm (slit-width 10 nm) at 37 °C. Kinetic analysis of initial velocities obtained was performed using the Henri-Michaelis-Menten equation for uncompetitive substrate inhibition $v = (V_{max} \times [S])/(K_m + [S] + [S]^2/K_i)$ and fit using the program GraFit. The iterative fits provided estimates of V_{max}, K_m and K_i and associated standard errors.

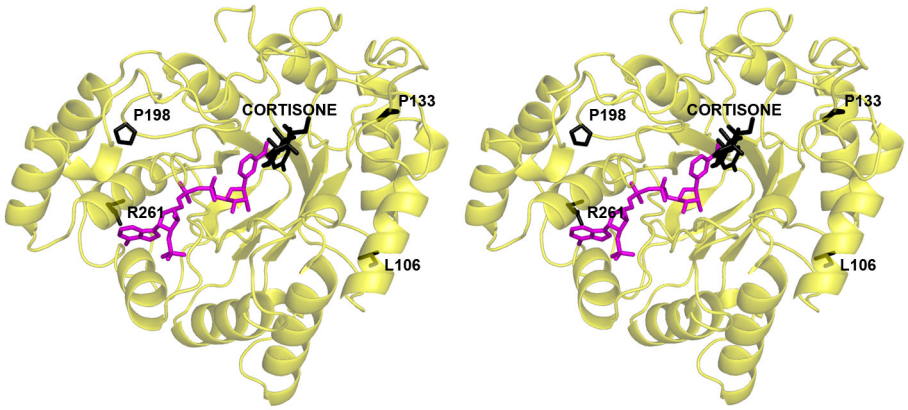

FIGURE 7. AKR1D1-NADP$^+$-cortisone complex: the positions of the natural mutations L106F, P198L, P133R, and R261C

Cortisone, L106, P198, P133, and R261 atoms are black, and NADP$^+$ atoms are magenta. Among these four residues, P133 in loop A is closest to the substrate binding site.

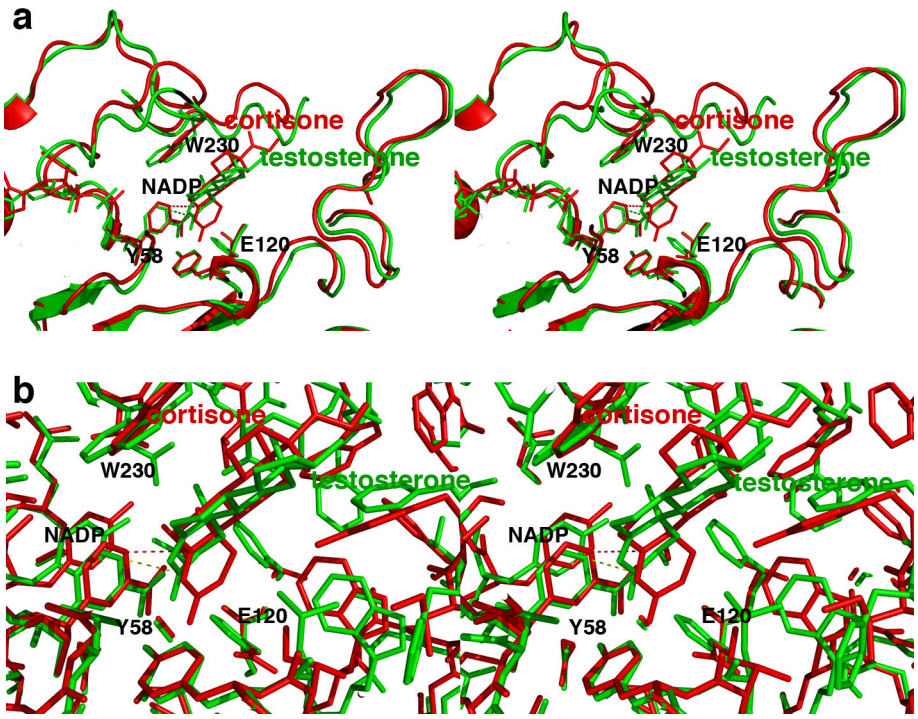

FIGURE 8. Comparisons of steroid binding modes in catalysis

(a) Superposition of the AKR1D1-$NADP^+$-cortisone complex (red) on the AKR1C9-$NADP^+$-testosterone complex (green) showing that the A ring of the substrate binds ~1 Å deeper in the active site of the former enzyme relative to the position of the nicotinamide ring of $NADP^+$. Presuming that NADPH binds similarly to $NADP^+$, the 4-pro-*R* hydride of NADPH would be adjacent to the substrate C3 carbonyl carbon in the AKR1C9 active site (green dotted line), whereas the 4-pro-*R* hydride of the NADPH cofactor would be adjacent to C5 of the substrate carbon-carbon double bond in the AKR1D1 active site (red dotted line). (b) Same orientation as (a), but a close-up view showing all atoms.

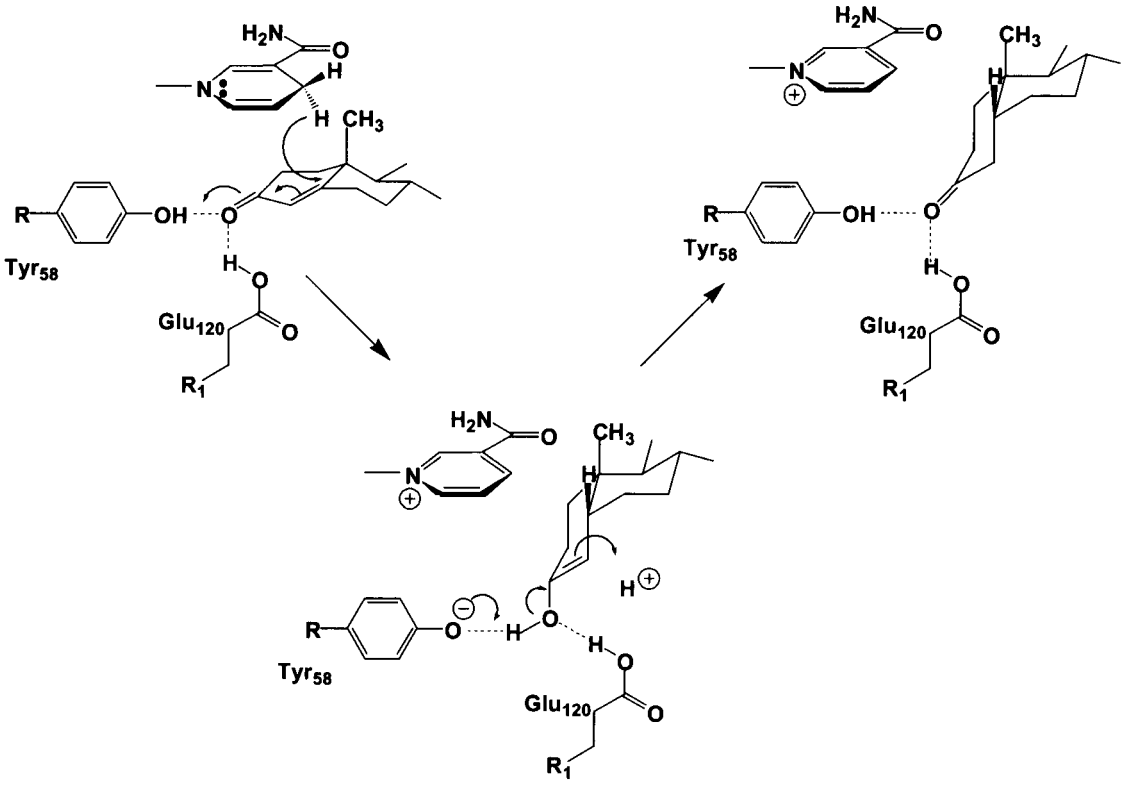

FIGURE 9. Proposed Catalytic Mechanism for Steroid Double-Bond Reduction

The 4-pro-*R* hydride transfer from the *re*-face of NADPH to the C5 position of the Δ^4-ene is proposed while the C3 carbonyl is polarized by both Tyr-58 and Glu-120, which create a "superacidic" oxyanion hole as predicted by Jez et al. (34).

Table 1

Data Collection and Refinement Statistics

Structure	AKR1D1-NADP$^+$-testosterone complex	AKR1D1-NADP$^+$-cortisone complex	AKR1D1-NADP$^+$-progesterone complex	AKR1D1-NADP$^+$-HEPES complex	AKR1D1-NADP$^+$ complex
PDB code	3BUR	3CMF	3COT	3BUV	3BV7
Resolution range, Å	50.0 - 1.62	50.0 - 1.90	30.0 - 2.03	50.0 - 1.35	50.0 - 1.79
Unique reflections measured	86,037 (7,952)	51,994 (4,640)	44,101 (4,301)	147,700 (13,665)	66,774 (6,684)
R_{merge} [a]	0.103 (0.36)[b]	0.112 (0.50)[b]	0.131 (0.58)[b]	0.094 (0.41)[b]	0.109 (0.39)[b]
I/σ(I)	20.3 (2.7)[b]	10.9 (2.5)[b]	12.2 (2.0)[b]	22.6 (1.9)[b]	20.5 (3.4)[b]
Completeness (%)	96.0 (90.0)[b]	93.7 (84.9)[b]	97.6 (96.9)[b]	95.7 (89.6)[b]	98.6 (100.0)[b]
Reflections used in refinement, test set	81,663/4,306	49,006/2,451	41,289/1,866	140,579/7,075	63,520/2,800
R/R_{free} [c]	0.228/0.248	0.195/0.223	0.194/0.234	0.218/0.232	0.236/0.257
Protein atoms[d]	5,254	5,254	5,254	5,254	5,254
Water molecules[d]	498	616	497	556	304
$NADP^+$ molecules[d]	2	2	2	2	2
Glycerol molecules[d]	10	-	-	2	3
Testosterone molecules[d]	2	-	-	-	-
Cortisone molecules[d]	-	2	-	-	-
Progesterone molecules[d]	-	-	2	-	-
HEPES molecules[d]	-	-	-	1	-
R.m.s. deviations					
Bond lengths, Å	0.007	0.006	0.007	0.005	0.012
Bond angles, °	1.1	1.2	1.1	1.2	1.1
Average B-factors, Å^2					
Main chain atoms	17	15	26	16	20
Side chain atoms	22	17	28	19	25
Water molecules	31	27	35	26	25
$NADP^+$	14	10	20	12	16
Testosterone	34	-	-	-	-
Cortisone	-	41	-	-	-
Progesterone	-	-	54	-	-
HEPES	-	-	-	34	-
Glycerol	42	-	-	43	41
Ramachandran statistics[e]					
Allowed (%)	90.4	89.2	89.0	89.9	91.1
Additionally allowed (%)	9.3	10.5	10.7	9.8	8.6
Generously allowed (%)	0.0	0.3	0.3	0.2	0.2
Disallowed (%)	0.2	0.0	0.0	0.2	0.2

[a] $R_{merge} = \Sigma| I-\langle I\rangle| /\Sigma I$, where I is the observed intensity and $\langle I\rangle$ is the average intensity calculated for replicate data.

[b] Number in parentheses refer to the outer 0.1 Å shell of data.

[c] Crystallographic R factor, $R = \Sigma(| F_O | - | F_C|)/\Sigma| F_O|$, for reflections contained in the working set. Free R factor, $R_{free} = \Sigma(| F_O| - | F_C|)/\Sigma| F_O|$, for reflections contained in the test set excluded from refinement. $| F_O|$ and $| F_C|$ are the observed and calculated structure factor amplitudes, respectively.

[d] Per asymmetric unit.

[e] Calculated with PROCHECK (50).